

RESEARCH PAPER

## Surface Morphology Engineering GQDs-decorated Metal-oxide Magnetic Composites for Radar Absorbing

Pooria Babaei, and Javad Safai-Ghomi \*

Department of Organic Chemistry, Faculty of Chemistry, University of Kashan, Kashan, I. R. Iran

### ARTICLE INFO

#### Article History:

Received 10 September 2023

Accepted 24 December 2023

Published 01 January 2024

#### Keywords:

Magnetic Composites

Metal-oxide

Radar Absorbing

Surface Morphology

### ABSTRACT

Nowadays, with the expanded radar (Radio Detection and Ranging) systems, the investigation of various materials with the capability to reduce or block reflected electromagnetic radiation has developed sharply. In this study, graphene quantum dots-decorated metal-oxide magnetic composites were fabricated as electromagnetic absorber materials because of their light weight, and good electric and magnetic properties. Furthermore, to investigate morphology engineering, a hydrothermal route was applied to fabricate nanostructures. Nanostructures were characterized by X-ray diffraction (XRD), scanning electron microscopy (SEM), Fourier transform infrared (FT-IR) spectroscopy, and elemental mapping (EDS-mapping). Also, the magnetic moment and electromagnetic interference shielding were tested by Vibrating-sample magnetometer (VSM) and reflection loss (RL), respectively.

### How to cite this article

Babaei P, Safai-Ghomi J. Surface Morphology Engineering GQDs-decorated Metal-oxide Magnetic Composites for Radar Absorbing. J Nanostruct, 2024; 14(1):83-92. DOI: 10.22052/JNS.2024.01.008

### INTRODUCTION

As a manifestation of energy, electromagnetic waves have special applications in our everyday life [1]. For instance, telecommunications systems, specialized medical equipment, solar radiation, etc. [2]. Among them, nanomaterials and developed composite have been considered in civilian, industrial, and military fields [3]. The radar systems were expanded during World War II and their development continues to the present day [4]. Therefore, it is necessary to use radar-absorbing material (RAM) to deal with radar systems. RAM plays the main role in controlling the electromagnetic environment [5]. The perfect RAM must have remarkable properties such as low cost [6], low density [7], good thermal stability [8], and strong attenuation capacity over a wide

frequency range [9, 10].

Nano-scale carbon materials such as carbon black [11], carbon nanotubes [12], carbon fibers [13], biomass carbon [14], graphite [15], and graphite-based materials [16, 17] have provided these features. Graphene quantum dots (GQDs) are graphene fragments that are small enough to cause exaction confinement and a quantum size effect [18]. These carbon nanostructures have low density, high thermal and electrical conductivity, outstanding physicochemical attributes, and optical transmittance [19].

Also, many reports have been published about the synergic effects of composites. Reports revealed that metal-oxide composites with various formulations are tunable for microwave absorption peaks [20]. Among these researches,

\* Corresponding Author Email: safaei@kashanu.ac.ir



the shape and size of the nanostructure play a key role in improving absorbing performances [21]. The hydrothermal route is a significant protocol for morphology engineering and nanomaterial preparation [22]. In fact, during the hydrothermal process, the conditions of the reaction (e.g. solvent type, temperature, pH adjuster, and molar ratio of precursors) are very important [23]. In other words, the morphology and size of the particles are controlled by the nucleation and grain growth process during the hydrothermal protocol [24]. In this current study, we have designed and fabricated nanoscale GQDs-decorated magnetic composites via a green, low-cost, and easy route (hydrothermal strategy) and the microwave absorbing performances were tested. Several nanocomposites with diverse morphologies were fabricated in various conditions (e.g. green routes, various pH adjusters, temperatures, etc.). Next, GQDs were applied to improve the surface. Due to further active sites on the surface of nanocomposites, morphology engineering can be

effective in microwave absorbing. Compared to pure magnetic composites, the GQDs-decorated magnetic composites presented excellent microwave absorbing performances in terms of both maximum reflection loss and the adsorption band width. Experimental data suggested that GQDs can find wide applications in the microwave-absorbing areas.

## MATERIALS AND METHODS

### Chemicals and typical procedures

The precursors were of analytical grade from Merck without extra purification. The as-prepared nanostructures were proved by Scanning electron microscope (SEM), X-ray diffraction analysis (XRD), Fourier transform infrared (FT-IR), Elemental mapping (EDS), and Value stream mapping (VSM) analysis.

### Fabrication of $Fe_3O_4$ spherical nanoparticles

Initially, 1 g of  $FeSO_4 \cdot 7H_2O$  and 0.72 g of  $Fe(NO_3)_3 \cdot 9H_2O$  were dissolved completely in

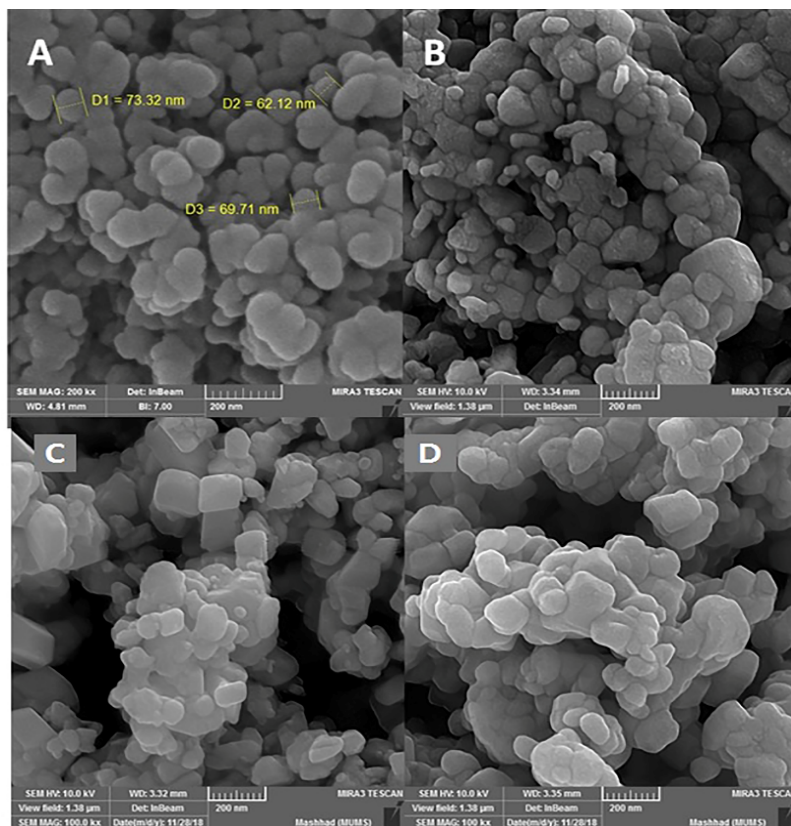


Fig. 1. SE-SEM images of  $Fe_3O_4$  NPs in the presence of (a) KOH (140 °C), (b)  $NH_3$  (140 °C), KOH (120 °C), and (d) KOH (160 °C).

distilled water to produce a 50 ml solution at ambient temperature. Under continuous stirring, the previously prepared base solution was added drop by drop to the above solution to bring pH=12. The solution directly got dark after the addition base solution and stirred at 25 °C (15

min). Eventually, the whole mixture was put in a 150 ml Teflon Lined stainless steel autoclave and transferred to an electric oven at 140 °C for 15 hours under hydrothermal conditions. The black solid was collected by an external magnetic field. The prepared Fe<sub>3</sub>O<sub>4</sub> nanoparticles were washed

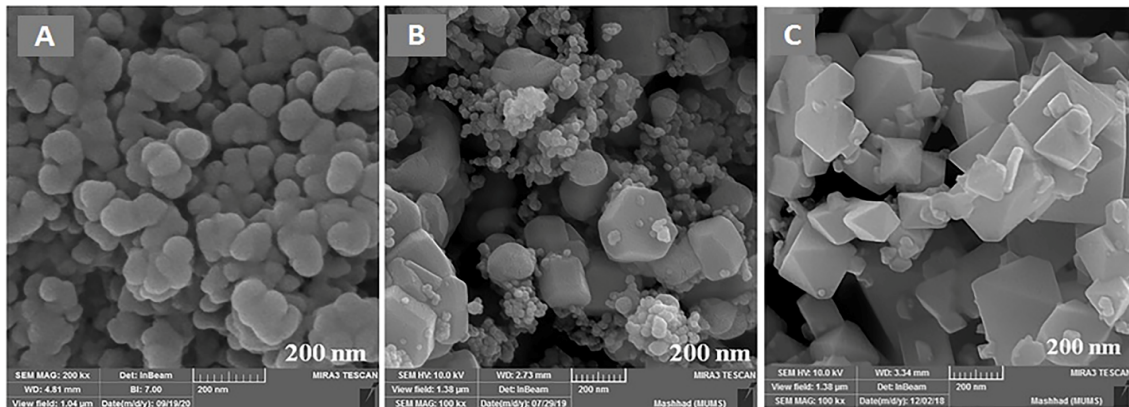


Fig. 2. FE-SEM images of CoFe<sub>2</sub>O<sub>4</sub> composite for 12 h (a) at 150 °C (KOH), (b) 180 °C (KOH), and 150 °C (NH<sub>3</sub>).

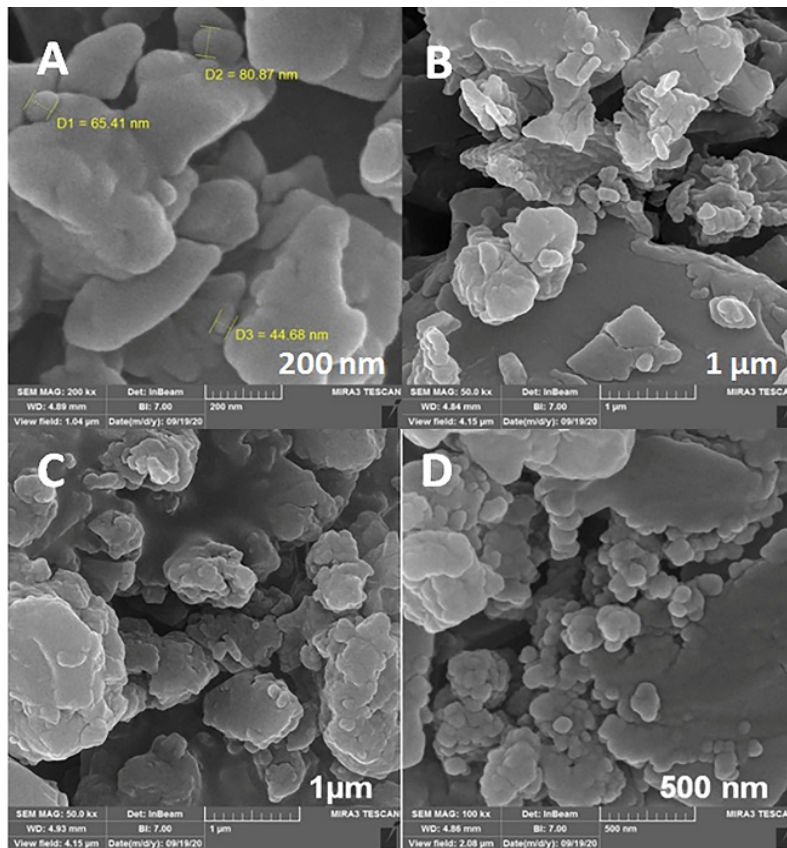


Fig. 3. FE-SEM images of Fe<sub>3</sub>O<sub>4</sub>/GQDs (a-b) and CoFe<sub>2</sub>O<sub>4</sub>/GQDs (c-d).

with dry ethanol and dried in a vacuum overnight at 65°C [19].

*Fabrication of CoFe<sub>2</sub>O<sub>4</sub> spherical nanocomposite*

FeSO<sub>4</sub>·7H<sub>2</sub>O (1 g), Fe(NO<sub>3</sub>)<sub>3</sub>·9H<sub>2</sub>O (0.72 g), and CoCl<sub>2</sub>·2H<sub>2</sub>O (0.59 g) were dissolved in 50 ml of distilled water at ambient temperature. Next, the as-prepared base solution was added droply to the above solution to bring pH=12 under continuous stirring. The mixture was stirred at 25 °C (15 min). Finally, the whole mixture was put in a 150 ml Teflon Lined stainless steel autoclave and transferred to an electric oven at 150 °C for 12 hours under hydrothermal conditions. The black solid was collected by an external magnetic field. The prepared CoFe<sub>2</sub>O<sub>4</sub> nanocomposites were washed with dry ethanol and dried in a vacuum overnight at 65°C [19].

*Fabrication of GQDs-decorated Fe<sub>3</sub>O<sub>4</sub> and CoFe<sub>2</sub>O<sub>4</sub> spherical nanocomposite*

The hydrothermal technique is the foremost

common route for the massive production of GQDs. The mixture of 1g of citric acid, 0.4 ml of ethylenediamine, and distilled water (50 cc) was mixed for 2 minutes (25 °C). Then, the as-fabricated Fe<sub>3</sub>O<sub>4</sub> or CoFe<sub>2</sub>O<sub>4</sub> magnetic nanostructures (1 g) were poured into the above mixture and sonicated for 2 min. Next, the mixture was put in a 150 ml Teflon Lined stainless steel autoclave and placed in the electric oven at 180 °C for 9 hours under hydrothermal conditions. At completion, the resulting sediment was collected under an external magnetic field and washed with dry ethanol. The separated precipitate, finally, dried at 55 °C for 24 hours under vacuum conditions [25].

**RESULTS AND DISCUSSION**

In general, there are various approaches to the fabrication of nanostructures which are sol-gel, microwave, precipitation, etc. [26]. Among them, the hydrothermal technique is an effective route fabrication and growth of advanced nanomaterials. In addition, engineering the structure morphology

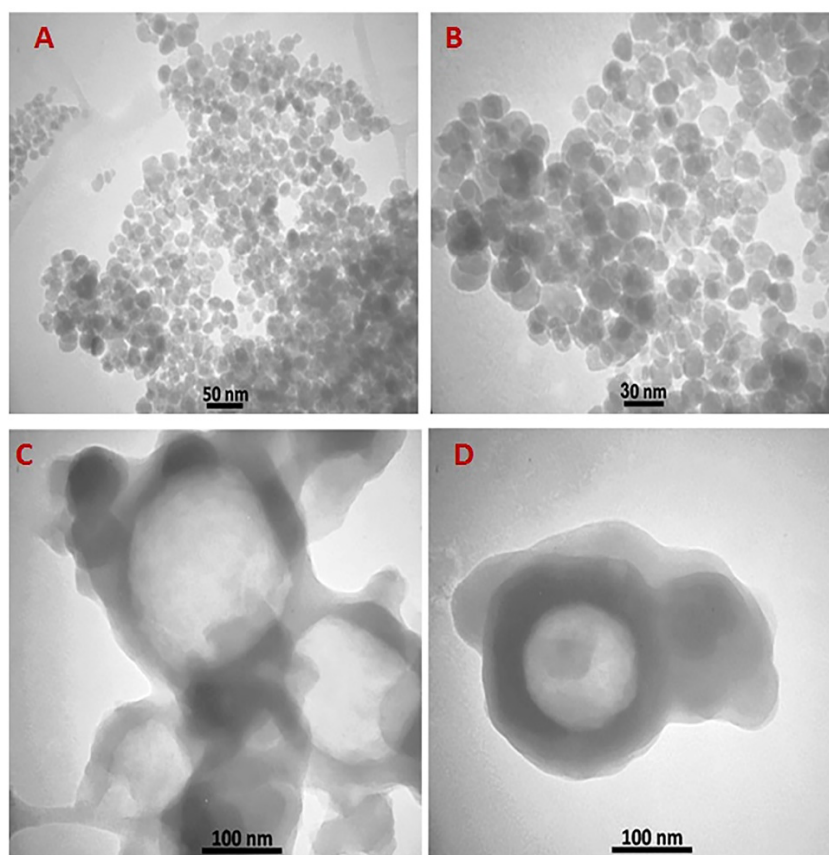


Fig. 4. TEM images of Fe<sub>3</sub>O<sub>4</sub>/GQDs (a-b) and CoFe<sub>2</sub>O<sub>4</sub>/GQDs (c-d).

(shape and size) plays a main role in structural properties. Besides, solvent, pH adjuster, reaction time, temperature, etc. are fundamental parameters in nanostructure size and morphology engineering [26, 27]. Moreover, many research papers have been reported about magnetic nanoparticles/composites. These nanostructures have been remarkably expanded because of their facile preparation, good performance, high stability, and high absorption [28]. In this study, the surface morphology of the  $\text{Fe}_3\text{O}_4$ ,  $\text{CoFe}_2\text{O}_4$ ,  $\text{Fe}_3\text{O}_4/\text{GQDs}$ , and  $\text{CoFe}_2\text{O}_4/\text{GQDs}$  were investigated by the FE-SEM route. In the case of  $\text{Fe}_3\text{O}_4$  NPs, KOH and  $\text{NH}_3(\text{aq})$  were used as pH adjusters. FE-SEM images of  $\text{Fe}_3\text{O}_4$  NPs in the presence of two different pH-adjusters are shown in Fig. 1. From Fig. 1a-b, the  $\text{Fe}_3\text{O}_4$  NPs could be recognized as having spherical and bulk shapes in the presence of KOH and  $\text{NH}_3(\text{aq})$  at 170 °C, respectively. As shown in Fig. 1c-d for appropriate morphology, the temperature was changed. Fig. 1c-d showed the formation of non-unique shapes at 120 and 160 °C, respectively.

FE-SEM images of the  $\text{CoFe}_2\text{O}_4$  composite are shown in Fig. 2. It is clear that the spherical and heterojunction shapes of the  $\text{CoFe}_2\text{O}_4$  composite were formed using KOH for 12 h at 150 °C and 180 °C, respectively (Fig. 2a-b). When the pH adjuster was changed to an ammonia solution, the spherical morphology was converted to a hexagonal shape at the same conditions (Fig. 2c).

Since GQDs can accommodate  $-\text{COOH}$  and  $-\text{OH}$  functional groups, their binding to magnetic nanostructures includes stability [29]. Fig. 3 exhibits the FE-SEM images of GQDs-decorated  $\text{Fe}_3\text{O}_4$  and  $\text{CoFe}_2\text{O}_4$  magnetic composites. As shown in Fig. 3 the  $\text{Fe}_3\text{O}_4$  and  $\text{CoFe}_2\text{O}_4$  spherical morphologies are changed after modification with GQDs. Also, for more investigation of  $\text{Fe}_3\text{O}_4/\text{GQDs}$  and  $\text{CoFe}_2\text{O}_4/\text{GQDs}$  NCs were applied. As can be seen in Fig. 4, the spherical structure of  $\text{Fe}_3\text{O}_4/\text{GQDs}$  and  $\text{CoFe}_2\text{O}_4/\text{GQDs}$  NCs were generated from dense nanosphere building blocks through the self-assembly process.

The XRD patterns of  $\text{Fe}_3\text{O}_4$ ,  $\text{CoFe}_2\text{O}_4$ ,  $\text{Fe}_3\text{O}_4/\text{GQDs}$

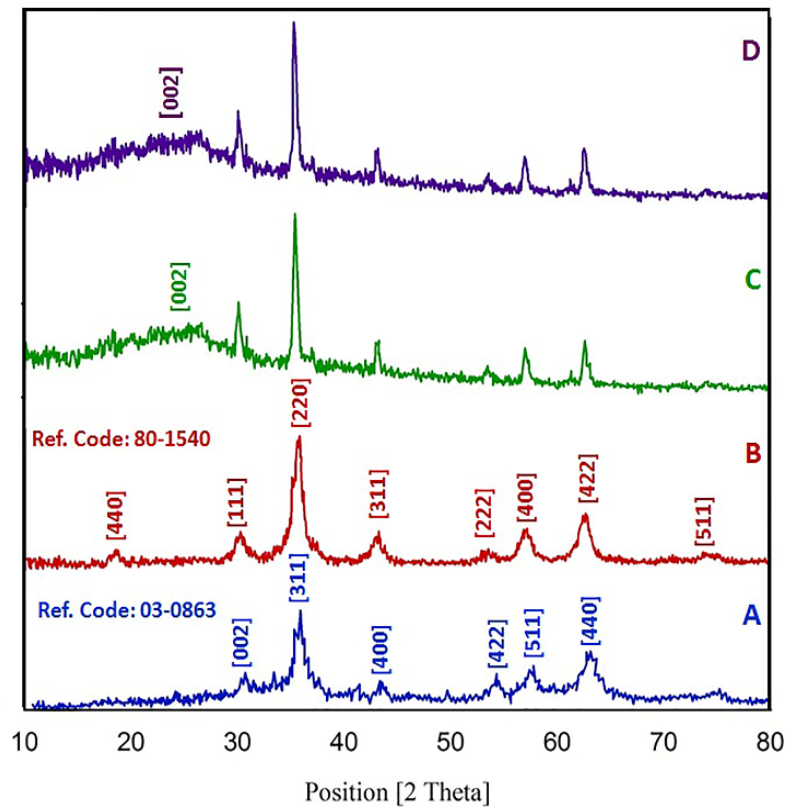


Fig. 5. XRD patterns of (a)  $\text{Fe}_3\text{O}_4$ , (b)  $\text{CoFe}_2\text{O}_4$ , (c)  $\text{Fe}_3\text{O}_4/\text{GQDs}$ , and (d)  $\text{CoFe}_2\text{O}_4/\text{GQDs}$  composites.

GQDs, and  $\text{CoFe}_2\text{O}_4/\text{GQDs}$  structures are illustrated in Fig. 5. As shown in Fig. 5a, the nano-sized  $\text{Fe}_3\text{O}_4$  Miller's index is seen; the intensity ratio and position of these peaks have admissible corresponding to the standard pattern (JCPDS No. 03-0863) [30]. According to the Debye formula ( $D = k\lambda/\beta\cos\theta$ ), the crystallite size was measured about 42 nm. To date, different papers have been reported about the XRD pattern of the  $\text{CoFe}_2\text{O}_4$  composite. The obtained XRD pattern in this study is totally in agreement with previous reports. The characteristic peaks can be observed in Fig. 5b that data match with reference code (JCPDS No. 80-1540) [31]. The  $\text{CoFe}_2\text{O}_4$  composite crystallite size, which is calculated by the Debye formula, was determined 56 nm. Investigation of the detailed XRD graph of the  $\text{CoFe}_2\text{O}_4$  composite has confirmed this description. In the case of Fig. 5c-d, a broad peak at  $2\theta=24^\circ$  is also related to the (002) plane corresponding to the presence of GQDs in

the magnetic nanostructure [32].

The FT-IR spectroscopy study of pure  $\text{Fe}_3\text{O}_4$  and  $\text{CoFe}_2\text{O}_4$  nanostructures have been exploited to achieve more exact data about the fabrication of GQDs decorated magnetic nanoparticles (Fig. 6). The absorption bands in the approximate region of  $509\text{ cm}^{-1}$  belong to Fe-O stretching vibration [33]. Two peaks at  $3423\text{ cm}^{-1}$  and  $1622\text{ cm}^{-1}$  also correspond to -OH stretching and bending vibration, respectively, due to absorbed  $\text{H}_2\text{O}$  by the surface  $\text{Fe}_3\text{O}_4$  nanoparticles (Fig. 6a). Based on the FT-IR spectrum of  $\text{CoFe}_2\text{O}_4$  composite represented in Fig. 6b, the two bands at  $509\text{ cm}^{-1}$  and  $1022\text{ cm}^{-1}$  are related to Fe-O and Co-Fe stretching vibration [34]. Compared to the Fig. 6a graph, new bands approximately at  $1072$ ,  $2858$ , and  $2989\text{ cm}^{-1}$  in the Fig. 6c spectrum are attributed to C=O,  $-\text{CH}_{\text{sp}2}$ , and  $-\text{CH}_{\text{sp}3}$  stretching vibration of GQDs [35]. Besides, the Fig. 6d spectrum shows that various peaks at  $600$ ,  $615$ ,  $780$ ,  $1388$ ,  $1680$ ,  $2920$ , and  $3385\text{ cm}^{-1}$

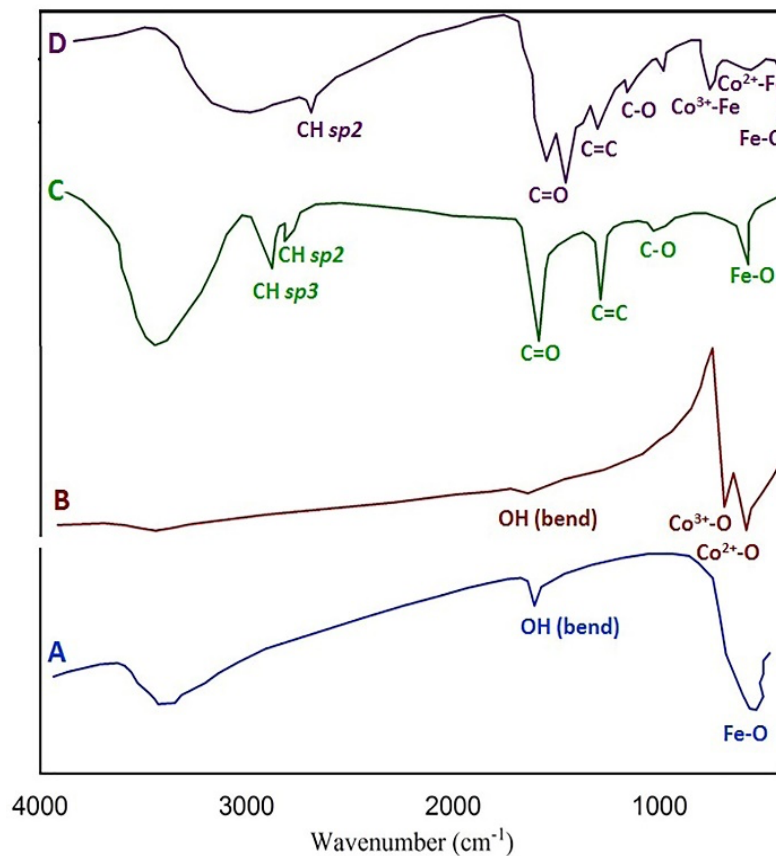


Fig. 6. FT-IR graphs of (a)  $\text{Fe}_3\text{O}_4$ , (b)  $\text{CoFe}_2\text{O}_4$ , (c)  $\text{Fe}_3\text{O}_4/\text{GQDs}$ , and (d)  $\text{CoFe}_2\text{O}_4/\text{GQDs}$  composites.

are related to Fe-O, Fe-Co<sup>2+</sup>, Fe-Co<sup>3+</sup>, C-O, C=O, -CH<sub>sp2</sub> and -CH<sub>sp3</sub> respectively.

Fig. 7 reveals the EDS analysis and elemental mapping of Fe<sub>3</sub>O<sub>4</sub>, CoFe<sub>2</sub>O<sub>4</sub>, Fe<sub>3</sub>O<sub>4</sub>/GQDs, and CoFe<sub>2</sub>O<sub>4</sub>/GQDs composites. In each case, the EDS patterns prove the presence of main elements

in nanostructures. Also, the percentage content of elements was tabulated in the EDS pattern. Moreover, the elemental mapping route depicted that all elements were well distributed in each nanostructure.

The magnetic properties of the as-fabricated

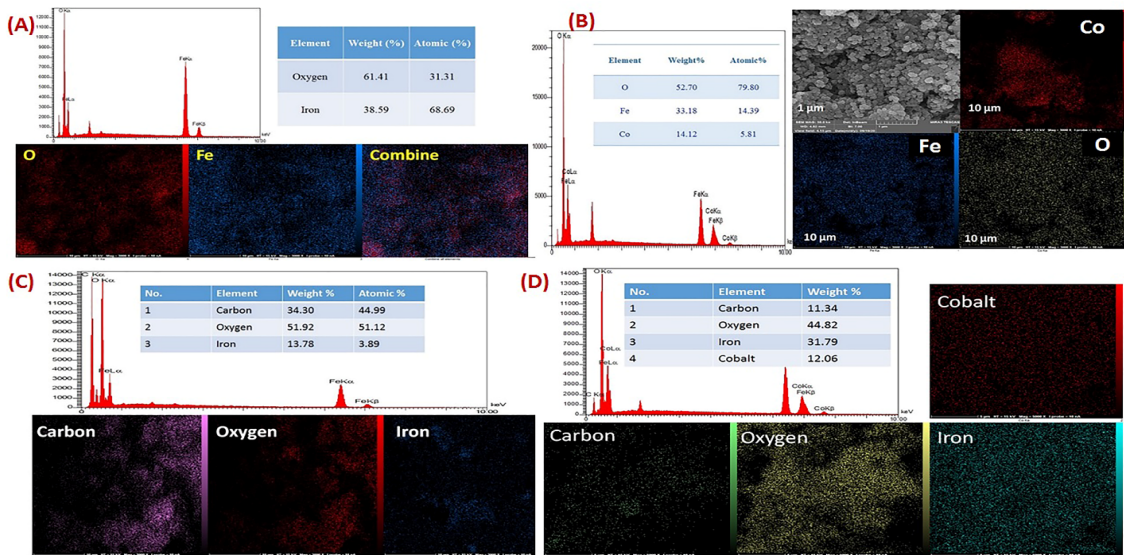


Fig. 7. EDS-mapping of (a) Fe<sub>3</sub>O<sub>4</sub>, (b) CoFe<sub>2</sub>O<sub>4</sub>, (c) Fe<sub>3</sub>O<sub>4</sub>/GQDs, and (d) CoFe<sub>2</sub>O<sub>4</sub>/GQDs composites.

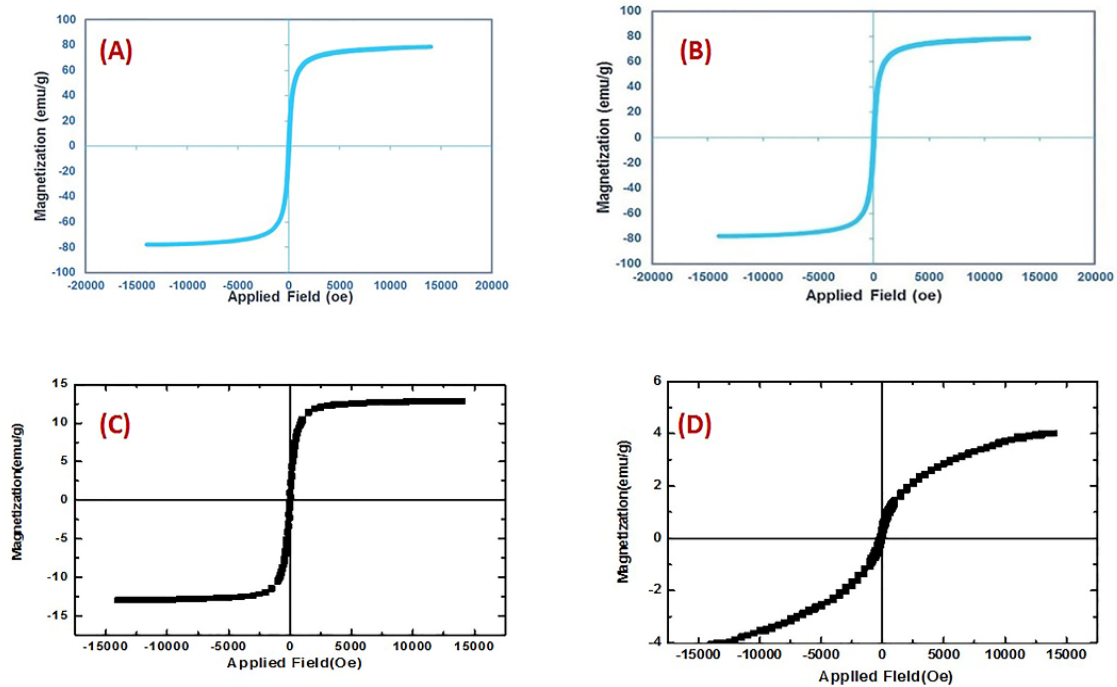


Fig. 8. VSM curves of (a) Fe<sub>3</sub>O<sub>4</sub>, (b) CoFe<sub>2</sub>O<sub>4</sub>, (c) Fe<sub>3</sub>O<sub>4</sub>/GQDs, and (d) CoFe<sub>2</sub>O<sub>4</sub>/GQDs composites.

$\text{Fe}_3\text{O}_4$ ,  $\text{CoFe}_2\text{O}_4$ ,  $\text{Fe}_3\text{O}_4/\text{GQDs}$ , and  $\text{CoFe}_2\text{O}_4/\text{GQDs}$  composites were measured by a VSM analysis at room temperature. The saturation magnetization ( $M_s$ ) values of the  $\text{Fe}_3\text{O}_4$  and  $\text{CoFe}_2\text{O}_4$  sphere composite are approximately 82 and 79 emu/g, respectively, which is suggestive of powerful magnetic attributes (Fig. 8a-b). The  $\text{Fe}_3\text{O}_4$  and  $\text{CoFe}_2\text{O}_4$  composites were decorated with GQDs. The magnetic attributes were reduced sharply (Fig. 8c-d). This change reveals that this decline could be a result of the existence of a non-magnetic layer. Therefore, the GQDs decorated magnetic composites were formed.

RL calculation for GQDs-decorated magnetic nanostructures with various concentrations of GQDs is shown in Fig. 9. Based on data, maximum absorption of microwave radiations for 5% and 10% of  $\text{Fe}_3\text{O}_4/\text{GQDs}$  NCs (2 mm thickness) were reported -19 and -26 dB, respectively, at a frequency of 0-20 GHz (Fig. 9a-b). Similarly, at a frequency of 0-20 GHz, maximum absorption of microwave radiations was registered at -17 and -27.5 dB for 5% and 10% of  $\text{CoFe}_2\text{O}_4/\text{GQDs}$  NCs with a thickness of 2 mm (Fig. 9c-d). The RL was increased with the increase of GQDs concentration. Moreover, the results showed that

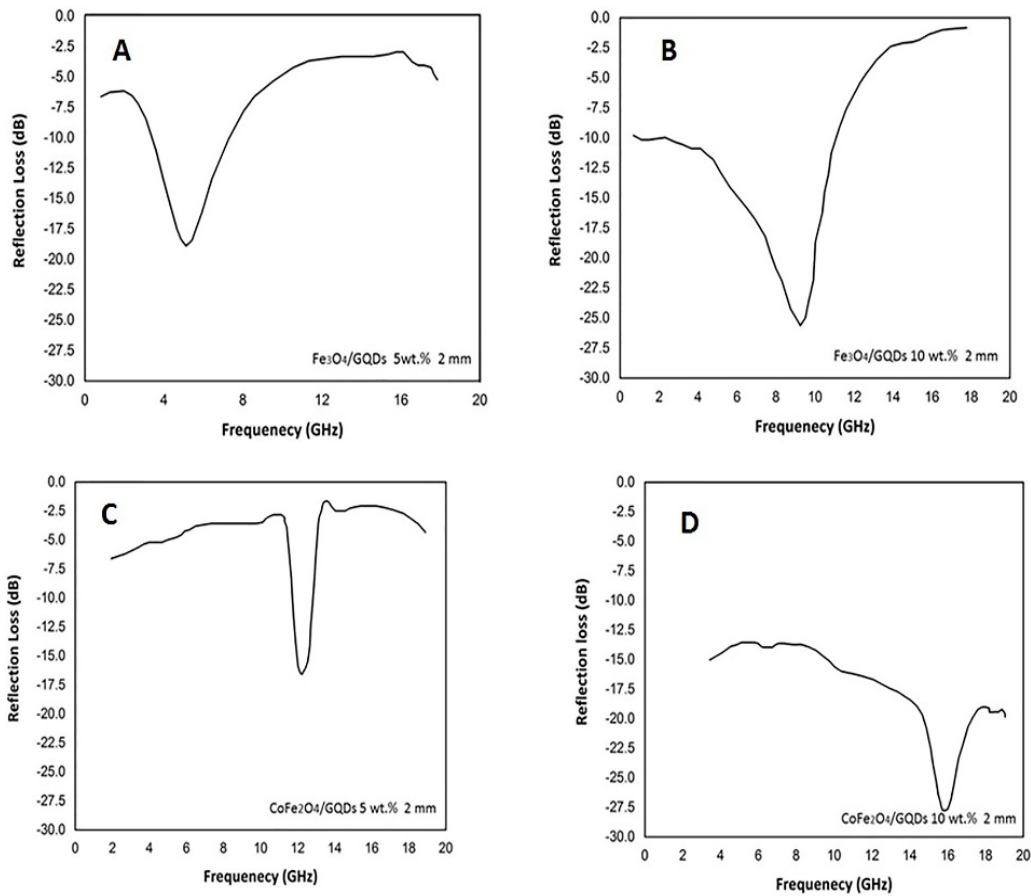


Fig. 9. RL curves of (a)  $\text{Fe}_3\text{O}_4/\text{GQDs}$  (5%), (b)  $\text{Fe}_3\text{O}_4/\text{GQDs}$  (10%), (c)  $\text{CoFe}_2\text{O}_4/\text{GQDs}$  (5%), and (d)  $\text{CoFe}_2\text{O}_4/\text{GQDs}$  (10%) composites.

Table 1. Comparison of the proposed nanocomposite with some materials for microwave absorbing.

No.	Materials	Reflection Loss (dB)	Frequency (GHz)	Thickness (mm)	Ref.
1	Graphene/Palates/Epoxy	-13.3	8-12	3	[3]
2	Mxenes derived laminated	-5.80	0-20	3	[36]
3	$\text{NiFe}_2\text{O}_4$ nanocomposite	-10	0-20	2	[1]
4	CNT/20%Fe	-21.5	5-50	3	[37]
5	$\text{Fe}_3\text{O}_4/\text{N-GQDs}$	-26	0-20	2	Our Job
6	$\text{CoFe}_2\text{O}_4/\text{N-GQDs}$	-27.5	0-20	2	Our Job

RL position changes in  $\text{Fe}_3\text{O}_4/\text{GQDs NCs}$  (from 5 to 9.5 GHz) and  $\text{CoFe}_2\text{O}_4/\text{GQDs NCs}$  (from 12 to 16 GHz), respectively.

Also, to compare the microwave absorbing of  $\text{N-GQDs/CoFe}_2\text{O}_4$  and  $\text{N-GQDs-Fe}_3\text{O}_4$  nanocomposites with reported other materials, we have summarized the results in Table 1.

## CONCLUSION

This study describes the design of microwave absorption magnetic nanostructures using GQDs based on surface morphology engineering. GQDs-decorated magnetic nanostructures were prepared via a hydrothermal route. The spherical shape was selected as the best morphology. The influence of spherical-shaped  $\text{Fe}_3\text{O}_4/\text{GQDs}$  and  $\text{CoFe}_2\text{O}_4/\text{GQDs}$  nanostructures on the reflection loss were investigated. The experimental results show that GQDs can increase the absorption of microwave radiation. Also, RL curves reveal that increasing GQDs concentration has a direct effect on increasing the absorption of microwave radiations.

## CONFLICT OF INTEREST

The authors declare that there is no conflict of interests regarding the publication of this manuscript.

## REFERENCE

- Ruiz-Perez F, López-Estrada SM, Tolentino-Hernández RV, Caballero-Briones F. Carbon-based radar absorbing materials: A critical review. *Journal of Science: Advanced Materials and Devices*. 2022;7(3):100454.
- Jia Z, Lan D, Lin K, Qin M, Kou K, Wu G, Wu H. Progress in low-frequency microwave absorbing materials. *Journal of Materials Science: Materials in Electronics*. 2018;29(20):17122-17136.
- Joy V, Padwal VG, Singh H, Nair RU. *EM Wave Propagation in Multilayered Radar Absorbing Structures (RAS). Optimization of Multilayered Radar Absorbing Structures (RAS) using Nature Inspired Algorithm*: CRC Press; 2021. p. 5-16.
- Zhang T, Zhang D, Shen M. A low-cost method for preliminary separation of reduced graphene oxide nanosheets. *Materials Letters*. 2009;63(23):2051-2054.
- Teng C-C, Ma C-CM, Lu C-H, Yang S-Y, Lee S-H, Hsiao M-C, et al. Thermal conductivity and structure of non-covalent functionalized graphene/epoxy composites. *Carbon*. 2011;49(15):5107-5116.
- Fang J, Zha W, Kang M, Lu S, Cui L, Li S. Microwave absorption response of nickel/graphene nanocomposites prepared by electrodeposition. *JMatS*. 2013;48(23):8060-8067.
- Patil AJ, Vickery JL, Scott TB, Mann S. Aqueous Stabilization and Self-Assembly of Graphene Sheets into Layered Bio-Nanocomposites using DNA. *Adv Mater*. 2009;21(31):3159-3164.
- Stankovich S, Dikin DA, Piner RD, Kohlhaas KA, Kleinhammes A, Jia Y, et al. Synthesis of graphene-based nanosheets via chemical reduction of exfoliated graphite oxide. *Carbon*. 2007;45(7):1558-1565.
- Li Y, Qin F, Quan L, Wei H, Luo Y, Wang H, Peng H-X. Vertical interphase enabled tunable microwave dielectric response in carbon nanocomposites. *Carbon*. 2019;153:447-457.
- Wang G, Zhang M, Liu S, Xie X, Ding G, Wang Y, et al. Synthesis of Layer-Tunable Graphene: A Combined Kinetic Implantation and Thermal Ejection Approach. *Adv Funct Mater*. 2015;25(24):3666-3675.
- Ansari A, Akhtar MJ. High porous carbon black based flexible nanocomposite as efficient absorber for X-band applications. *Materials Research Express*. 2018;5(10):105017.
- Wang Y, Gao X, Wu X, Luo C. Facile synthesis of Mn<sub>3</sub>O<sub>4</sub> hollow polyhedron wrapped by multiwalled carbon nanotubes as a high-efficiency microwave absorber. *Ceram Int*. 2020;46(2):1560-1568.
- Min D, Zhou W, Qing Y, Luo F, Zhu D. Highly oriented flake carbonyl iron/carbon fiber composite as thin-thickness and wide-bandwidth microwave absorber. *Journal of Alloys and Compounds*. 2018;744:629-636.
- Cheng Y, Seow JZY, Zhao H, Xu ZJ, Ji G. A Flexible and Lightweight Biomass-Reinforced Microwave Absorber. *Nanomicro Lett*. 2020;12(1):125-125.
- Du X, Wang B, Mu C, Wen F, Xiang J, Nie A, Liu Z. Facile Synthesis of Carbon-Encapsulated Ni Nanoparticles Embedded into Porous Graphite Sheets as High-Performance Microwave Absorber. *ACS Sustainable Chemistry & Engineering*. 2018;6(12):16179-16185.
- Zhao H, Han X, Li Z, Liu D, Wang Y, Wang Y, et al. Reduced graphene oxide decorated with carbon nanopolyhedrons as an efficient and lightweight microwave absorber. *Journal of Colloid and Interface Science*. 2018;528:174-183.
- Lu WB, Wang JW, Zhang J, Liu ZG, Chen H, Song WJ, Jiang ZH. Flexible and optically transparent microwave absorber with wide bandwidth based on graphene. *Carbon*. 2019;152:70-76.
- Safardoust-Hojaghan H, Salavati-Niasari M. Degradation of methylene blue as a pollutant with N-doped graphene quantum dot/titanium dioxide nanocomposite. *Journal of Cleaner Production*. 2017;148:31-36.
- Babaei P, Safaei-Ghomi J. Engineered N-doped graphene quantum dots/ $\text{CoFe}_2\text{O}_4$  spherical composites as a robust and retrievable catalyst: fabrication, characterization, and catalytic performance investigation in microwave-assisted synthesis of quinoline-3-carbonitrile derivatives. *RSC Adv*. 2021;11(55):34724-34734.
- Mahanta UJ, Gogoi JP, Borah D, Bhattacharyya NS. Dielectric characterization and microwave absorption of expanded graphite integrated polyaniline multiphase nanocomposites in X-band. *ITDEI*. 2019;26(1):194-201.
- Zhang N, Huang Y, Zong M, Ding X, Li S, Wang M. Synthesis of ZnS quantum dots and  $\text{CoFe}_2\text{O}_4$  nanoparticles co-loaded with graphene nanosheets as an efficient broad band EM wave absorber. *Chem Eng J*. 2017;308:214-221.
- Denkbaşı EB, Çelik E, Erdal E, Kavaz D, Akbal Ö, Kara G, Bayram C. Magnetically based nanocarriers in drug delivery. *Nanobiomaterials in Drug Delivery*: Elsevier; 2016. p. 285-331.
- Tabish TA, Zhang S. *Graphene Quantum Dots: Syntheses, Properties, and Biological Applications*. *Comprehensive Nanoscience and Nanotechnology*: Elsevier; 2016. p. 171-

- 192.
24. Sanjeev Kumar R, Veeravazhuthi V, Vishnu Shankar D, Muthukumarasamy N, Thambidurai M. Influence of cobalt concentration on structural and optical properties of ZnS quantum dots. *Journal of Sol-Gel Science and Technology*. 2014;71(1):152-158.
  25. Babaei P, Safaei-Ghomi J. L-proline covered N doped graphene quantum dots modified CuO/ZnO hexagonal nanocomposite as a robust retrievable catalyst in synthesis of substituted chiral 2-amino-4H-chromenes. *Materials Chemistry and Physics*. 2021;267:124668.
  26. Safardoust-Hojaghan H, Salavati-Niasari M, Amiri O, Rashki S, Ashrafi M. Green synthesis, characterization and antimicrobial activity of carbon quantum dots-decorated ZnO nanoparticles. *Ceram Int*. 2021;47(4):5187-5197.
  27. Babaei P, Safai-Ghomi J, Rashki S. Engineered dual-purpose Ta-doped ZnO/Hydroxyapatite nanocomposites: Antibacterial activity and robust catalyst in MW-Induced synthesis of chromopyrimidines. *Ceram Int*. 2022;48(6):8359-8373.
  28. Babaei P, Safaei-Ghomi J, Rashki S, Mahmoudi Kharazm A. Morphology modified by polyvinylpyrrolidone for enhanced antibacterial and catalytic execution of bioactive Ag/ZnO composites based on hydroxyapatite in the synthesis of O-Aminocarbonitriles. *Ceram Int*. 2023;49(14):22826-22836.
  29. Safaei-Ghomi J, Babaei P, L-proline-linked N-GQDs/ZnO/CuO Chiral Retrievable Catalyst: Synthesis, Characterization, and Investigation of Catalytic Performance in Diastereoselective Synthesis of Furocoumarin Natural Products, *Journal of Nanostructures*, 2021; 11; 711-727.
  30. Raktshah J. A comprehensive review on the synthesis, characterization, and catalytic application of transition-metal Schiff-base complexes immobilized on magnetic Fe<sub>3</sub>O<sub>4</sub> nanoparticles. *Coord Chem Rev*. 2022;467:214614.
  31. Vishwas M, Venkatesha Babu KR, Arjuna Gowda KV, Babu Gandla S. Synthesis, characterization and photo-catalytic activity of magnetic CoFe<sub>2</sub>O<sub>4</sub> nanoparticles prepared by temperature controlled co-precipitation method. *Materials Today: Proceedings*. 2022;68:497-501.
  32. Akbarian P, Kheirmand M, Faraji M. Facile electrochemical fabrication of high-performance graphene quantum dots-supported Mn<sub>3</sub>O<sub>4</sub>/Ag hybrid catalyst for oxygen reduction reaction in alkaline media. *IJER*. 2022;46(15):23004-23019.
  33. Nouri K, Ghassemzadeh M, Mohsenzadeh F, Afsharpour M. Imidazolium organometallic complex of palladium on Fe<sub>3</sub>O<sub>4</sub> nanoparticles as selective and magnetically recoverable nanocatalyst for C-C cross-coupling reactions. *Appl Organomet Chem*. 2023;37(5).
  34. Das S, Das MM, Dhamodharan P, Manoharan C. Dielectric, magnetic and electrochemical characterization of CoFe<sub>2</sub>O<sub>4</sub> nanoparticles and their application as an anode material in Li-ion battery. *Inorg Chem Commun*. 2022;145:110050.
  35. Mokhtari A, Yavari A, Khatamian M, Sadeghi E, Peighambari NS, Aydemir U. Facile synthesis of graphene quantum dots/ZSM-5 type metalosilicate composites and evaluating their performance in photocatalytic degradation of methylene blue and electrochemical water splitting. *Adv Powder Technol*. 2023;34(1):103892.
  36. Feng W, Luo H, Wang Y, Zeng S, Tan Y, Deng L, et al. Mxenes Derived Laminated and Magnetic Composites with Excellent Microwave Absorbing Performance. *Sci Rep*. 2019;9(1):3957-3957.
  37. Hussein MI, Jehangir SS, Rajmohan IJ, Haik Y, Abdulrehman T, Clément Q, Vukadinovic N. Microwave Absorbing properties of metal functionalized-CNT-polymer composite for stealth applications. *Sci Rep*. 2020;10(1):16013-16013.